Eur. Phys. J. A **31**, 804–809 (2007)
DOI 10.1140/epja/i2006-10290-6

THE EUROPEAN PHYSICAL JOURNAL A

Special Article – QNP 2006

Exploring the details of the QCD phase diagram

Ph. de Forcrand[1,2] and O. Philipsen[3,a]

[1] Institut für Theoretische Physik, ETH Zürich, CH-8093 Zürich, Switzerland
[2] CERN, Physics Department, TH Unit, CH-1211 Geneva 23, Switzerland
[3] Institut für Theoretische Physik, Westfälische Wilhelms-Universität Münster, Germany

Received: 22 December 2006
Published online: 22 March 2007 –

Abstract. We summarize our recent results on the phase diagram of QCD with $N_f = 2 + 1$ quark flavors, as a function of temperature T and quark chemical potential μ. Using staggered fermions, lattices with temporal extent $N_t = 4$, and the exact RHMC algorithm, we first determine the critical line in the quark mass plane $(m_{u,d}, m_s)$ where the finite-temperature transition at $\mu = 0$ is second order. We confirm that the physical point lies on the crossover side of this line. Our data are consistent with a tricritical point at $(m_{u,d}, m_s) = (0, \sim 500)$ MeV. Then, using an imaginary chemical potential, we determine in which direction this second-order line moves as the chemical potential is turned on. Contrary to standard expectations, we find that the region of first-order transitions shrinks in the presence of a chemical potential, which is inconsistent with the presence of a QCD critical point at small chemical potential. The emphasis is put on clarifying the translation of our results from lattice to physical units, and on discussing the apparent contradiction of our findings with earlier lattice studies. Finally, we review related results obtained via simulations at fixed baryon number via the canonical ensemble.

PACS. 12.38.Gc Lattice QCD calculations – 12.38.Mh Quark-gluon plasma

1 Introduction

In recent years, considerable efforts have been devoted to the determination of the phase diagram of QCD at finite temperature and density [1]. At zero chemical potential, the nature of the quark hadron phase transition depends on the quark masses $m_{u,d}$ and m_s, and the qualitative expectations are summarized in fig. 1. In the limits of zero and infinite quark masses (lower left and upper right corners), order parameters corresponding to the breaking of a symmetry can be defined, and one finds numerically that a first-order transition takes place at a finite temperature T_c. On the other hand, one observes an analytic crossover at intermediate quark masses. Hence, each corner must be surrounded by a region of first-order transition, bounded by a second-order line as in fig. 1. The line in the heavy-quark corner has been studied in [2]. Here, we want to determine the chiral critical line.

Along both lines, the universality class has been numerically determined to be that of the $3d$ Ising model. With this knowledge at hand, a powerful observable to determine the critical couplings is the Binder cumulant $B_4 \equiv \langle \delta X^4 \rangle / \langle \delta X^2 \rangle^2$, where $\delta X = X - \langle X \rangle$, and we take for X the u, d quark condensate $\bar{\psi}\psi$. In the infinite volume limit and when evaluated at the (pseudo-)critical temperature, this observable takes on the values 1 or 3 when the phase change corresponds to a first-order transition or a crossover, respectively, while it assumes the value $B_4 = 1.604$ characteristic for the $3d$ Ising universality class on a second-order critical point.

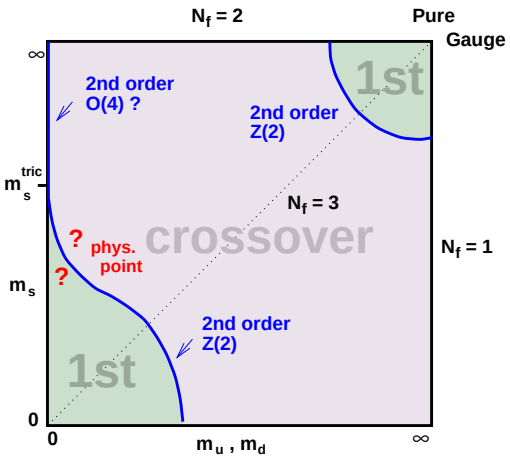

Fig. 1. Schematic phase transition behaviour of $N_f = 2 + 1$ flavor QCD for different choices of quark masses $(m_{u,d}, m_s)$, at $\mu = 0$ (from [1]).

[a] e-mail: ophil@uni-muenster.de

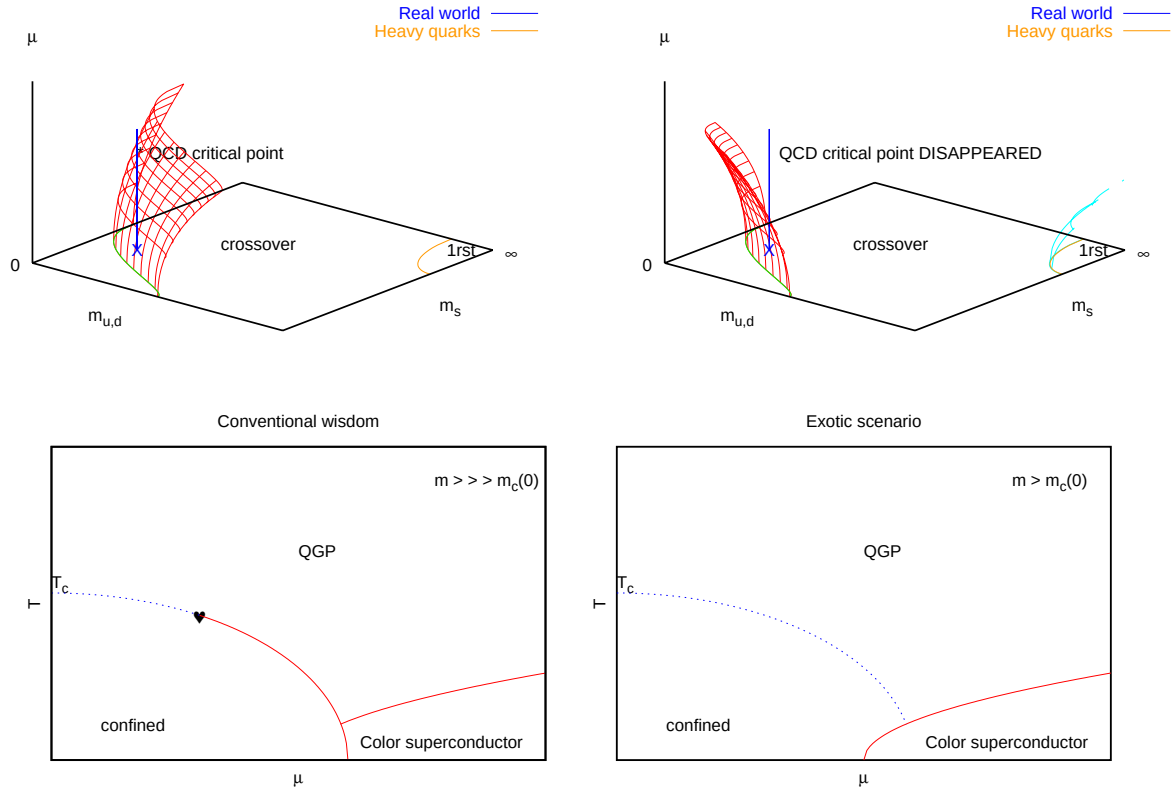

Fig. 2. Upper panel: the chiral critical surface in the case of positive (left) and negative (right) curvature. If the physical point is in the crossover region for $\mu = 0$, a finite μ phase transition will only arise in the scenario (left) with positive curvature, where the first-order region expands with $|\mu|$. Note that for heavy quarks, the first-order region shrinks with $|\mu|$ (right) [5]. Lower panel: phase diagrams for fixed quark mass (here $N_f = 3$) corresponding to the two scenarios depicted above.

On lattices $8^3, 12^3$ and $16^3 \times 4$, we thus estimate the critical couplings as those for which $B_4 = 1.604$. For each mass point $(m_{u,d}, m_s)$, we accumulate at least 200k RHMC trajectories, and interpolate among 4 or more $m_{u,d}$ values to find the critical $m_{u,d}$ mass m^c at previously fixed m_s. We obtain the set of points in fig. 4, left.

We then consider the effect of a baryonic chemical potential, $\mu_B = 3\mu$. As a function of quark chemical potential μ, represented vertically in fig. 2, the critical line determined at $\mu = 0$ now spans a surface. The standard expectation for the QCD phase diagram is depicted in fig. 2 left. The first-order region expands as μ is turned on, so that the physical point, initially in the crossover region, eventually belongs to the critical surface. At that chemical potential μ_E, the transition is second order: that is the QCD critical point. Increasing μ further makes the transition first order. Drawn in the (T, μ)-plane, this corresponds to the standard expected diagram fig. 2, left. A completely different scenario arises if instead the first-order region shrinks as μ is turned on. In that case (fig. 2, right), the physical point remains in the crossover region for any μ.

Since the phenomenologically interesting question is whether a QCD critical point (μ_E, T_E) exists at small $\mu_E, \mu_E/T_E \lesssim 1$, *i.e.* for $\mu_B \lesssim 500\,\mathrm{MeV}$, this question can be addressed by simulations with an imaginary chemical potential, followed by an analytic continuation based on a Taylor expansion [3,4]. The benefit of using an imaginary chemical potential is that the fermion determinant is positive in this case, hence there is no sign problem and simulations are technically equally feasible as those for $\mu = 0$. Using this approach, we determine the curvature $\frac{\mathrm{d}m^c}{\mathrm{d}\mu^2}|_{\mu=0}$ of the critical surface at $\mu = 0$. We find that it is negative, so that the first-order region shrinks as in fig. 2, right. Note that in the opposite corner, the first-order region also shrinks [5].

Section 2 tests our methodology in the $N_f = 3$ case. Section 3 describes the $N_f = 2 + 1$ study. Section 4 compares our results with earlier lattice studies and discusses the various limitations of our approach.

2 $N_f = 3$

We first check our methodology in the case of 3 degenerate flavors. This is basically a repeat of ref. [6], this time using the RHMC algorithm [7] instead of the R algorithm.

The RHMC algorithm eliminates the stepsize error of the R algorithm, which differs in magnitude in the chirally symmetric and broken phases [8]. As a result, the value of $m^c(\mu = 0)$ is considerably different: $(am^c(\mu = 0))$ moves from 0.033(1) (R algorithm) [6] to 0.0260(5) (see fig. 3, left). We have checked, by performing zero-temperature

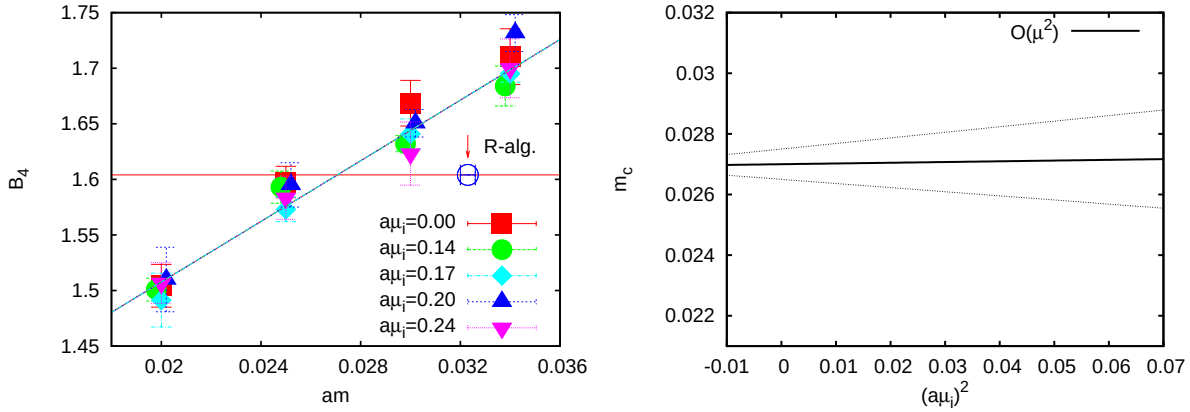

Fig. 3. Left: $B_4(am, a\mu_I)$ for different imaginary chemical potentials. Right: one-sigma error band for the critical mass $am^c(a\mu_I)$ resulting from a linear fit.

simulations at this quark mass, that this is not a simple renormalization effect, but that the physical ratio m_π/T_c is lowered by about 10%. Therefore, an exact algorithm appears mandatory for the study of the $N_f = 2+1$ critical line. Moreover, RHMC turns out to be vastly more efficient, by up to a factor 20 in our case for the smallest quark masses [9].

We now turn on an imaginary chemical potential $\mu = i\mu_I$, and for each μ_I monitor the Binder cumulant B_4 as a function of the quark mass. Our results are summarized in fig. 3, left. The chemical potential has almost no influence on B_4. A lowest-order fit, linear in am and $(a\mu)^2$, gives the error band in fig. 3, right, corresponding to

$$am^c(a\mu) = 0.0270(5) - 0.0024(160)(a\mu)^2. \qquad (1)$$

Care must be taken for the conversion to physical units. The crucial point is that, as we increase the chemical potential μ_I, we tune the gauge coupling β upwards to maintain criticality, so that $a(\beta)$ decreases: our observation that $am^c(\mu_I) \approx$ const does *not* mean that $m^c(\mu_I) \approx$ const, but that $m^c(\mu_I)$ increases with μ_I, or *decreases* with a real chemical potential μ. If we express

$$\frac{am^c(\mu)}{am^c(0)} = 1 + \frac{c_1'}{am^c(0)}(a\mu)^2 + \ldots, \qquad (2)$$

$$\frac{m^c(\mu)}{m^c(0)} = 1 + c_1\left(\frac{\mu}{\pi T}\right)^2 + \ldots \qquad (3)$$

then c_1 and c_1' are related by

$$c_1 = \frac{\pi^2}{N_t^2}\frac{c_1'}{am^c(0)} + \left(\frac{1}{T_c(m,\mu)}\frac{\mathrm{d}T_c(m,\mu)}{\mathrm{d}(\mu/\pi T)^2}\right)_{\mu=0}, \qquad (4)$$

where $m = m^c(\mu)$ in the second term. Writing the transition temperature as

$$\frac{T_c(m,\mu)}{T_c(m_0^c,0)} = 1 + A\frac{m-m_0^c}{\pi T} + B\left(\frac{\mu}{\pi T}\right)^2 + \ldots \qquad (5)$$

one obtains

$$c_1 = \left(B + \frac{\pi^2}{N_t^2}\frac{c_1'}{am^c(0)}\right)\left(1 - A\frac{m_0^c}{\pi T}\right)^{-1}. \qquad (6)$$

c_1' and $\frac{m_0^c}{\pi T}$ are both small, so that c_1 is nearly equal to B. Estimates of B and A can be obtained by converting our result for the pseudo-critical gauge coupling

$$\beta_0(am, a\mu) = 5.1369(3) + 1.94(3)(am - am_0^c) + 0.781(7)(a\mu)^2 \qquad (7)$$

to physical units. Using the 2-loop β-function gives $A = 2.111(17), B = -0.667(6)$ so that finally

$$\frac{m^c(\mu)}{m^c(0)} = 1 - 0.7(4)\left(\frac{\mu}{\pi T}\right)^2 + \ldots. \qquad (8)$$

The error above is conservative and includes the uncertainty from using different fitting forms (see [10], table 2). The main source of systematic error comes from using the 2-loop β-function to obtain B. The non-perturbative β-function varies more steeply and may increase A and B, in magnitude, by up to a factor 2. This will make c_1 more negative.

We thus have clear evidence that, in the $N_f = 3$ theory on an $N_t = 4$ lattice, the region of first-order transitions *shrinks* as a baryon chemical potential is turned on, and the "exotic scenario" of fig. 2, right, is the correct one. This result is further supported by recent simulations of the same theory, under an isospin chemical potential [11].

3 $N_f = 2 + 1$

We now proceed to the non-degenerate case. First, at $\mu = 0$, we map out the line of second-order transitions in the $(am_{u,d}, am_s)$-plane. Our results, shown fig. 4, left, are in qualitative agreement with expectations fig. 1. In particular, they are consistent with the possible existence of a tricritical point ($m_{u,d} = 0, m_s = m_s^{tric}$). Using its known, Gaussian exponents, our data favor (blue on-line line in fig. 4, left) a heavy $m_s^{tric} \sim 2.8T_c$.

A more immediate issue is whether the QCD physical point lies on the crossover side of the critical line as expected. For that purpose, we have performed spectrum calculations at $T \sim 0$, at the parameters corresponding to

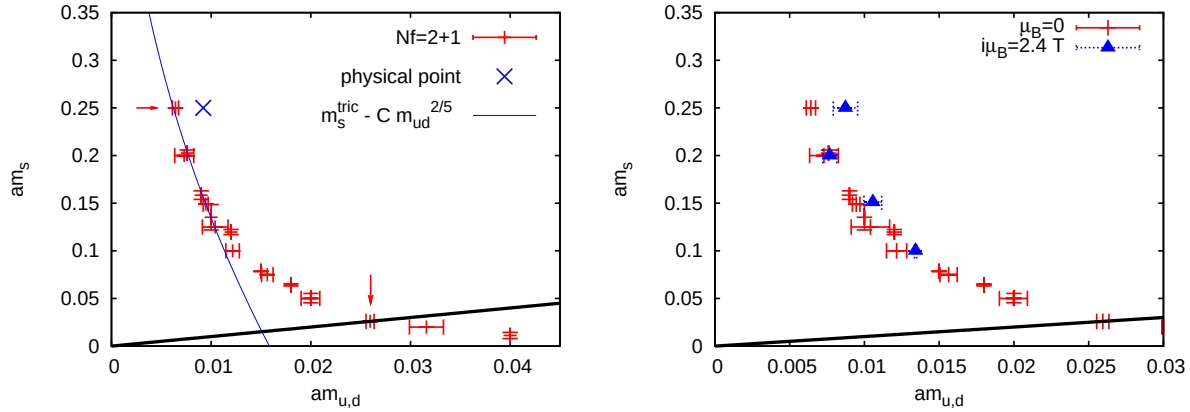

Fig. 4. Left: the chiral critical line in the bare quark mass plane at $\mu = 0$. $N_f = 3$ is shown by the thick solid line. Also shown are the physical point according to [12], and a fit corresponding to a tricritical point $m_s^{tric} \sim 2.8T_c$. Right: comparison of the critical line at $\mu = 0$ and $a\mu_I = 0.2$.

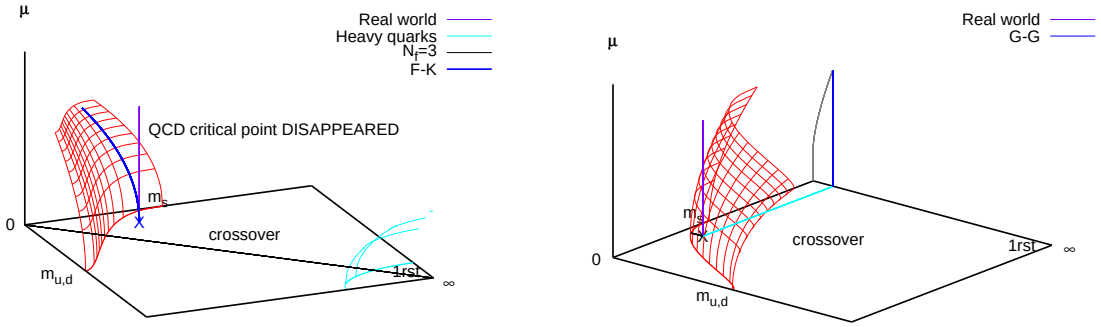

Fig. 5. Left: effect of keeping the quark mass fixed in lattice units in [12]. Right: comparison at finite μ between the $N_f = 2+1$ and the $N_f = 2$ theory considered in [16].

the horizontal arrow in fig. 4, left ($am_{u,d} = 0.005, am_s = 0.25, \beta = 5.1857$). They show that m_s is approximately tuned to its physical value ($\frac{m_K}{m_\rho} \sim \frac{m_K}{m_\rho}|_{phys}$), while the pion is lighter than in QCD ($\frac{m_\pi}{m_\rho} = 0.148(2) < 0.18$). This confirms that the physical point lies on the right of the critical line, *i.e.* in the crossover region[1]. This conclusion has been confirmed by very recent calculations on finer lattices [13]. Also, we find T_c to vary little along the critical line, in accordance with model calculations [14].

We now couple an imaginary chemical potential $a\mu_I = 0.2$ to the two light flavors, and measure the change in the critical mass $am_{u,d}$ as in the $N_f = 3$ case. Figure 4, right, shows the same trend as for $N_f = 3$: the critical mass is constant or slightly increasing, *in lattice units*. The conversion to physical units proceeds as in eqs. (2)–(8). Since the critical gauge coupling $\beta_0(a\mu_I)$ increases with μ_I, the coefficient B, which is the dominant contribution to c_1, is negative. Together with a very small or slightly negative value for c_1', it implies again that the first-order region *shrinks* as the baryon chemical potential is turned on, and the "exotic scenario" of fig. 2, right, is the correct one.

[1] In fact, our estimate of the lattice parameters corresponding to the physical point is consistent with that of Fodor and Katz using the same action, but the R algorithm [12].

This statement comes with several caveats: i) our lattice is very coarse ($a \sim 0.3$ fm); ii) as we consider lighter $m_{u,d}$, our box becomes small ($m_\pi L \sim 1.7$ for the worst case); iii) we use "rooting" of the staggered determinant to simulate 1 and 2 flavors, albeit our measure is positive with an imaginary μ, so that we avoid the pitfalls of [15].

4 Discussion

Our results appear in qualitative contradiction with those of Fodor and Katz [12] and of Gavai and Gupta [16], which both conclude for the existence of a critical point (μ_E, T_E) at small chemical potential $\mu_E/T_E \lesssim 1$. Let us consider the reasons for such disagreement.

– Fodor and Katz obtain Monte Carlo results at $\beta = \beta_c, \mu = 0$, and perform a double reweighting in (β, μ) along the pseudo-critical line $\beta_c(a\mu)$. By construction, this reweighting is performed at a quark mass fixed *in lattice units*: $am_{u,d} = \frac{m_{u,d}}{T_c} = \text{const}$. Since the critical temperature T_c decreases as they turn on μ, so does their quark mass. This decrease of the quark mass pushes the transition towards first order, which might be the reason why they find a critical point at small μ. This effect is illustrated in the sketch fig. 5, left, where the bent trajectory

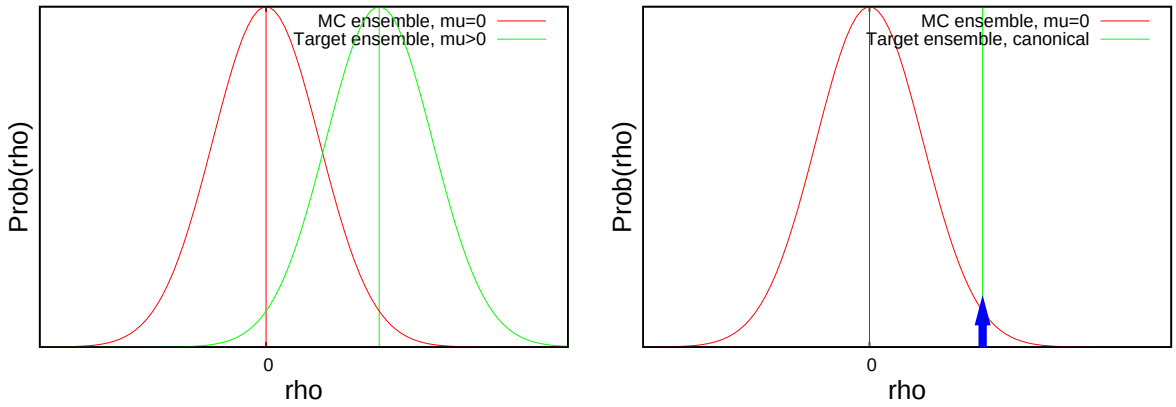

Fig. 6. (Colour on-line) Left: the Monte Carlo ensemble produces a distribution of baryon densities ρ (red) centered about $\rho = 0$, to be reweighted according to the desired, target ensemble (green) centered about $\rho > 0$. Very little large-ρ information is available. Right: by chosing the target ensemble to be canonical, one alleviates the need for large-ρ information, thus increasing the reliability of the results.

à la Fodor and Katz intersects the critical surface, while the vertical line of constant physics does not.

Put another way, Fodor and Katz measure the analogue of eq. (2) instead of (3). From their fig. 1 (ref. [12]), the coefficient c_1' which one would extract would be essentially zero like ours. As in our case, the variation of T_c with μ makes a dominant contribution, which might change the results qualitatively.

– Gavai and Gupta try to infer the location of the critical point by estimating the radius of convergence of the Taylor expansion of the free energy in $(\mu/\pi T)^2$. Regardless of the systematic error attached to such an estimate when only 4 Taylor coefficients are available, we want to point out that they consider a theory without strange quark, *i.e.* $N_f = 2$ only. The (μ, T) phase diagram of such a theory is qualitatively different from that of $N_f = 2 + 1$ QCD. At $\mu = 0$, the order of the finite-temperature transition as $m_{u,d} \to 0$ is not settled [17]. Assuming a second-order $O(4)$ transition, one expects then a tricritical point at $(m_{u,d} = 0, \mu = \mu^{tric})$, beyond which a non-zero critical mass $m^c_{u,d}(\mu)$ can be defined, as sketched in fig. 5, right. The quantitative relevance of results, even accurate, for this $N_f = 2$ theory to QCD is unclear to us.

Therefore, we find no inconsistency between our results and those above. We conclude that the existence of a critical point (μ_E, T_E) in QCD at small chemical potential $\mu_E/T_E \lesssim 1$ is an open question. Our numerical evidence, with the caveats mentioned in sect. 3, is that the curvature of the critical surface is as illustrated fig. 2, right. Our main systematic error comes from our coarse lattice spacing $a \sim 0.3\,\mathrm{fm}$ [18]. If confirmed on a finer lattice, the implications of our finding would be as follows. In the region where a leading Taylor expansion of the critical surface is a good approximation, *i.e.* $\mu/T \lesssim 1$, corresponding to the experimentally accessible regime, no critical point exists which is analytically connected to $\mu = 0$. Of course, we cannot exclude that the QCD phase diagram is more complex, and partly inaccessible to our imaginary μ + Taylor expansion strategy. In particular this leaves open the possibility of a critical point *not* analytically connected to the one at $\mu = 0$.

5 Canonical approach

The canonical ensemble, where the baryon density is fixed instead of the conjugate chemical potential, provides a potentially fruitful approach to the study of QCD at finite density. Its theoretical advantage is illustrated in fig. 6. The ensemble of configurations sampled from the Monte Carlo ensemble, whatever this ensemble is chosen to be, has a distribution of baryon densities ρ centered around $\rho = 0$, illustrated by the Gaussian-like red on-line curve in fig. 6. By reweighting with a factor $\propto \exp(\mu/TV\rho)$, one attempts to obtain information on the target, $\mu \neq 0$ ensemble, which has a distribution of baryon densities illustrated by the Gaussian-like green on-line curve, centered around $\rho \neq 0$. When the volume V is increased, the red and green on-line curves both become narrower Gaussians, and an *overlap* problem appears: the Monte Carlo ensemble contains very little information relevant to the target ensemble, and correct results can only be maintained by increasing statistics exponentially with V. The problem is particularly acute for the large-density tail of the target ensemble. By changing the target ensemble to canonical, *i.e.* with a fixed baryon density as illustrated by the blue on-line delta-function in fig. 6, one eliminates the need to include high-density information. Thus, while the canonical ensemble does not provide a cure to the sign and overlap problems, there is some reason to expect that it delivers more reliable results than the usual reweighting to the grand-canonical ensemble, up to larger volumes or average baryon densities.

Reweighting of the $\mu = 0$ ensemble to the canonical one has been performed in ref. [19], in a pilot project with $N_f = 4$ degenerate flavors of staggered quarks, on a small $6^3 \times 4$ lattice. A selection of results is presented in fig. 7.

Figure 7 (left) shows, as a function of the baryon density, the derivative of the free-energy density with

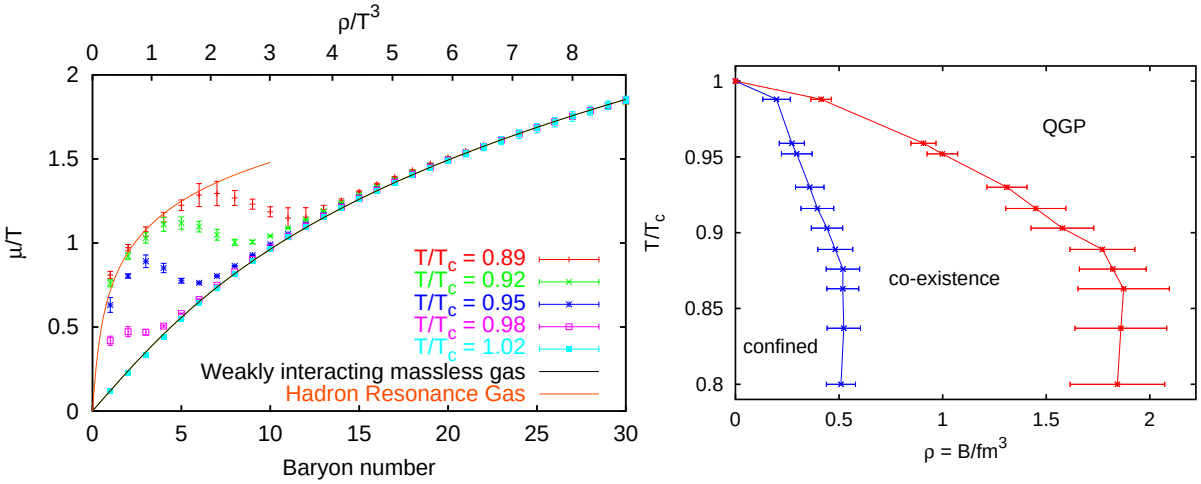

Fig. 7. Results from the canonical-ensemble approach [19]. Left: equivalent chemical potential *versus* baryon density. Right: boundaries of the coexistence region, obtained from the left panel by a Maxwell construction.

respect to the baryon density. This quantity is equal to the baryon chemical potential, in the saddle point approximation which is exact in the thermodynamic limit. Note that reliable results are obtained for systems containing up to 30 baryons, and chemical potentials up to $\mu/T \sim 2$. For the chosen quark mass $m_q/T = 0.2$, a first-order transition takes place between the confining and the plasma phases. The transition is visible in the S-shape of the data, indicating multiple solutions for the baryon density at a given chemical potential. A Maxwell construction reveals the critical chemical potential $\mu_c(T)$, and the limits $\rho_1(T), \rho_2(T)$ of the coexistence region. The latter are shown in fig. 7 (right) as a function of temperature. One sees that the pure hadronic phase has a maximum baryon density of about 0.5 baryon/fm^3, which is not too far from the real-world nuclear density of 0.17 baryon/fm^3. The minimum density in the plasma phase is about 6 quarks/fm^3.

By choosing a heavier quark mass, one can ensure that the $\mu = 0$ transition becomes a crossover. If a critical point exists at some finite $\mu = \mu_E$, the transition will become first-order for $\mu > \mu_E$, which will be evidenced by the appearance of an S-shaped curve in fig. 7 (left) for $\mu > \mu_E$ only. While these simulations are still performed on a small volume, which causes important systematic errors in the estimate of the critical couplings and of the order of the phase transition, comparison with the imaginary-μ approach of the previous sections, and with the reweighting approach of Fodor and Katz [12] will provide a valuable crosscheck.

References

1. E. Laermann, O. Philipsen, Annu. Rev. Nucl. Part. Sci. **53**, 163 (2003) [arXiv:hep-ph/0303042]; O. Philipsen, PoS (LAT2005) 016 (2006); PoS (JHW2005) 012 (2006) [arXiv:hep-lat/05100677].
2. P. Hasenfratz, F. Karsch, I.O. Stamatescu, Phys. Lett. B **133**, 221 (1983); C. Alexandrou *et al.*, Phys. Rev. D **60**, 034504 (1999) [arXiv:hep-lat/9811028]; A. Dumitru, D. Roder, J. Ruppert, Phys. Rev. D **70**, 074001 (2004) [arXiv:hep-ph/0311119].
3. P. de Forcrand, O. Philipsen, Nucl. Phys. B **642**, 290 (2002) [arXiv:hep-lat/0205016].
4. M. D'Elia, M.P. Lombardo, Phys. Rev. D **67**, 014505 (2003) [arXiv:hep-lat/0209146].
5. S. Kim *et al.*, PoS (LAT2005) 166 (2006) [arXiv:hep-lat/0510069].
6. P. de Forcrand, O. Philipsen, Nucl. Phys. B **673**, 170 (2003) [arXiv:hep-lat/0307020].
7. M.A. Clark *et al.*, Nucl. Phys. Proc. Suppl. **140**, 835 (2005) [arXiv:hep-lat/0409133].
8. J.B. Kogut, D.K. Sinclair, arXiv:hep-lat/0504003.
9. M.A. Clark *et al.*, PoS (LAT2005) 115 (2006) [arXiv:hep-lat/0510004].
10. P. de Forcrand, O. Philipsen, arXiv:hep-lat/0607017.
11. D.K. Sinclair, J.B. Kogut, arXiv:hep-lat/0609041.
12. Z. Fodor, S.D. Katz, JHEP **0404**, 050 (2004) [arXiv:hep-lat/0402006].
13. Y. Aoki, G. Endrodi, Z. Fodor, S.D. Katz, K.K. Szabo, Nature **443**, 675 (2006).
14. Z. Szep, PoS (JHW2005) 017 (2006) [arXiv:hep-ph/0512241].
15. M. Golterman, Y. Shamir, B. Svetitsky, Phys. Rev. D **74**, 071501 (2006) [arXiv:hep-lat/0602026].
16. R.V. Gavai, S. Gupta, Phys. Rev. D **71**, 114014 (2005) [arXiv:hep-lat/0412035].
17. J.B. Kogut, D.K. Sinclair, Phys. Rev. D **73**, 074512 (2006) [arXiv:hep-lat/0603021]; M. D'Elia, A. Di Giacomo, C. Pica, Phys. Rev. D **72**, 114510 (2005) [arXiv:hep-lat/0503030].
18. F. Karsch *et al.*, Nucl. Phys. Proc. Suppl. **129**, 614 (2004) [arXiv:hep-lat/0309116].
19. P. de Forcrand, S. Kratochvila, PoS (LAT2005) 167 (2006) [arXiv:hep-lat/0509143]; Nucl. Phys. Proc. Suppl. **153**, 62 (2006) [arXiv:hep-lat/0602024].